Dark Matter Constraints from Planck Observations of the Galactic Polarized Synchrotron Emission

Silvia Manconi,[1,*] Alessandro Cuoco,[2,3] and Julien Lesgourgues[1]
[1]*Institute for Theoretical Particle Physics and Cosmology, RWTH Aachen University, Sommerfeldstraße 16, 52056 Aachen, Germany*
[2]*Dipartimento di Fisica, Università di Torino, via P. Giuria, 1, I-10125 Torino, Italy*
[3]*Istituto Nazionale di Fisica Nucleare, Sezione di Torino, Via P. Giuria 1, 10125 Torino, Italy*

(Received 19 April 2022; accepted 27 July 2022; published 9 September 2022)

Dark matter (DM) annihilation in our Galaxy may produce a linearly polarized synchrotron signal. We use, for the first time, synchrotron polarization to constrain the DM annihilation cross section by comparing theoretical predictions with the latest polarization maps obtained by the Planck satellite collaboration. We find that synchrotron polarization is typically more constraining than synchrotron intensity by about 1 order of magnitude, independently of uncertainties in the modeling of electron and positron propagation, or of the Galactic magnetic field. Our bounds compete with cosmic microwave background limits in the case of leptophilic DM.

DOI: 10.1103/PhysRevLett.129.111103

Introduction.—High-energetic cosmic-ray (CR) electrons *and* positrons ($e^{\pm}$ in what follows) can be either accelerated in primary sources such as supernova remnants and pulsar wind nebulae, or produced by spallation of hadronic CRs. Besides, CR $e^{\pm}$ might also be produced by the annihilation or decay of dark matter (DM) particles in the Galactic DM halo. Relativistic $e^{\pm}$ then gyrate and propagate in the interstellar Galactic magnetic field (GMF), and produce secondary emissions such as radio and microwave emissions through the synchrotron process. The synchrotron signal of DM origin has been extensively investigated in the past using many radio and microwave surveys, such as the Wilkinson Microwave Anisotropy Probe (WMAP) and Planck, finding constraints that are complementary to other probes both for the Galactic halo [1–10] and extragalactic targets [11–18]. Previous DM searches focused on the synchrotron total intensity, i.e., the Stokes parameter I. However, synchrotron emission of relativistic $e^{\pm}$ is partially linearly polarized, and a signal in polarization amplitude (i.e., Stokes P) is thus expected. We here exploit for the first time the Planck polarization maps in order to constrain Galactic DM signals. Polarization data have also been used together with total intensity data to study Galactic synchrotron emission and constrain CR propagation and large scale GMF models in absence of DM annihilation; see, e.g., Refs. [19–30].

The total intensity and the polarization properties of the DM synchrotron emission depend on the strength and orientation of the GMF, as well as on the spatial and energetic distribution of CR $e^{\pm}$ produced by DM. As we shall detail in what follows, the synchrotron intensity and polarization signals are complementary, since they are controlled by different properties of the GMF. We thus expect them to be affected by different systematic uncertainties.

Microwave maps.—The Planck instrument measures both the intensity and polarization of the microwave and submillimeter sky, in terms of the Stokes components I (intensity) and Q, U (polarization). The polarization amplitude is defined as $P = \sqrt{Q^2 + U^2}$. In particular, Planck has so far provided the deepest and highest-resolution view of the microwave and submillimeter sky by mapping anisotropies in the cosmic microwave background (CMB) radiation. This made it possible to put strong constraints on the standard cosmological model and its possible variations [31].

The Planck sky maps contain contributions from the CMB as well as many other astrophysical components ranging from compact Galactic and extragalactic sources to diffuse backgrounds as synchrotron and free-free emission in our Galaxy; see, e.g., Fig. 4 in Ref. [31]. Here, we are interested in constraining a possible diffuse signal coming from DM annihilation in our Galaxy that, depending on the DM properties, may contribute significantly to the diffuse background. Since the CMB contribution is well-measured, we consider CMB-subtracted maps. We refrain from modeling and subtracting any other contribution from the diffuse backgrounds, such as the Galactic synchrotron emission. We thus derive conservative DM constraints requiring that the DM signal does not exceed the observed emission, once the CMB contribution has been subtracted.

We use data products corresponding to the third release by the Planck Collaboration for the low frequency instruments (LFI) at 30, 44, and 70 GHz. Regarding the polarization emission, this Planck Collaboration release supersedes all

© 2022 American Physical Society

previous releases thanks to significantly lower contamination from systematic errors [32]. CMB-subtracted maps can be obtained using multifrequency information. We use the maps processed with the Needlet Internal Linear Combination (NILC) method [32], which still contain all the diffuse backgrounds.

They can be downloaded from the Planck legacy archive [33] with a resolution of $\mathrm{Nside} = 1024$ [34] in the HEALPix pixelization scheme [35]. This corresponds to a mean spacing between adjacent pixels of about 0.06°. For each frequency, the downloaded files contain three maps, one for each of the three Stokes parameters I, Q, and U. These maps contain the observed blackbody differential brightness temperature [36] in units of K_{CMB}, which is connected to the Rayleigh-Jeans (RJ) differential brightness temperature in K_{RJ} by a conversion formula that also accounts for color and leakage corrections based on instrument bandpass; see Ref. [28] for more details.

Before comparing the DM predicted P map with observations, we need to build the experimental P map and its error map from the available Q and U maps. This is achieved with the following steps: (i) *Smoothing*. We first smooth the CMB-subtracted I, Q, U maps with a Gaussian beam of 1° FWHM in order to increase the signal-to-noise ratio and reduce systematic effects caused by beam asymmetries. We then create a polarization amplitude map defined as $P = \sqrt{Q^2 + U^2}$, keeping the original NSide resolution of the Q, U maps. The resulting I and P full-sky maps at 30 GHz are shown in the upper panels of Fig. 1. We provide the full-sky maps at 44 and 70 GHz in the Supplemental Material [37]. (ii) *Error estimation*. For the purpose of obtaining robust DM constraints, we need to build error maps from the I, Q, U maps themselves. We estimate the error at each pixel as the variance of all neighboring pixels up to 0.5°, while sticking to the native NSide resolution. This provides an estimate of the noise except in the vicinity of point sources [43]. The error map for P is derived from the Q, U error maps using error propagation. The resulting sky maps for σ_I (σ_P) for 30 GHz are illustrated in the left (right) lower panel of Fig. 1. One can see by eye that error maps follow the scanning pattern of Planck: the error is smaller where the instrument observes longer and vice versa. (iii) *Degrading*. If needed, the above maps are degraded to a larger pixel resolution. While this is straightforward for the I, P maps, for the error maps one needs to take into account that the error scales

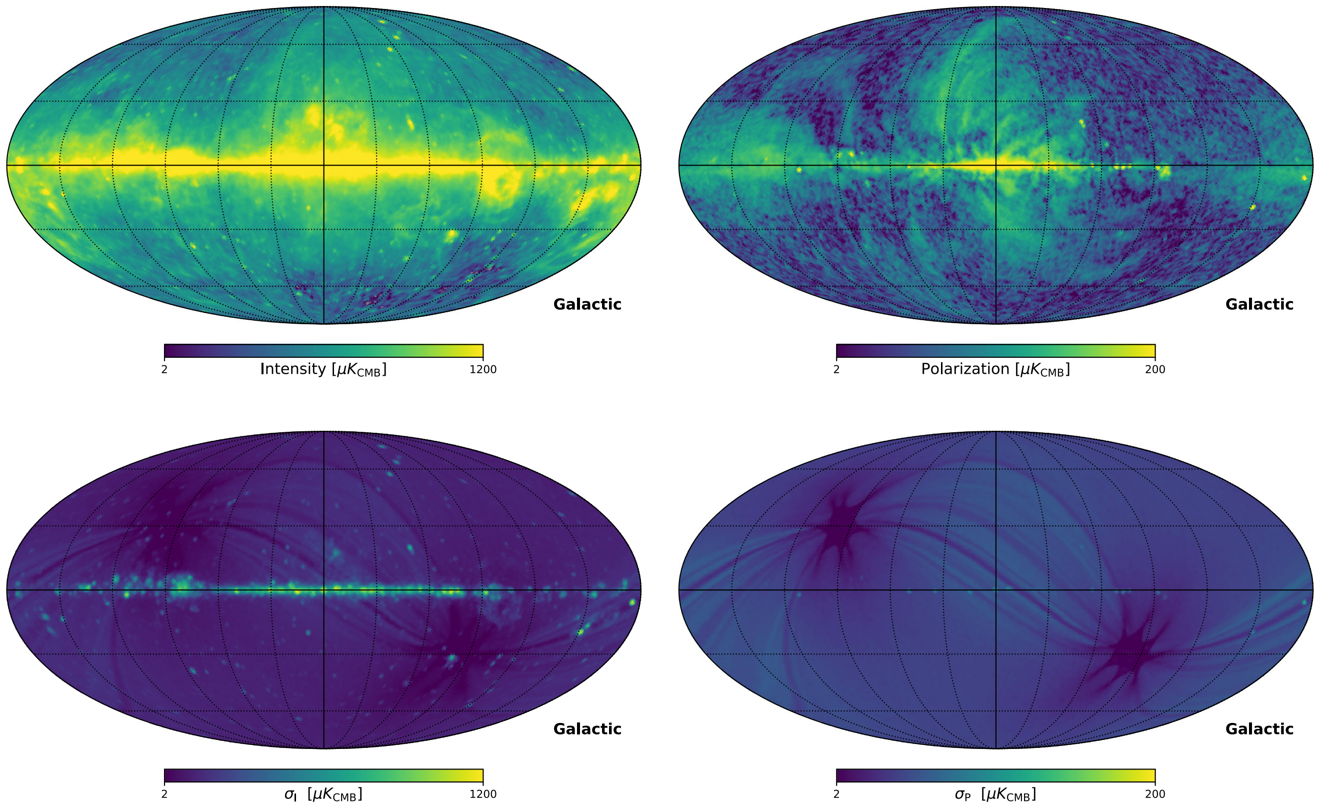

FIG. 1. Planck 30 GHz data and error estimate (σ). Upper row:NILC CMB-subtracted foreground maps after smoothing with FWHM of 1° and degrading the resolution to $\mathrm{NSide} = 64$, for the Stokes intensity (I, left) and polarization (P, right). Lower row: Error estimate for I (left) and P (right); see text for details. All maps are shown in a Mollweide projection and with a logarithmic color mapping. The minimum and maximum values are manually set to highlight the map structures on top of the noise.

with the pixel size. Going from NSide 1024 to a generic lower resolution l, we have $\sigma_P^l = \sigma_P/\sqrt{N_{\rm pix}^{1024}/N_{\rm pix}^l}$.

Synchrotron from Galactic dark matter.—We consider weekly interacting massive particles (WIMPs) as benchmark DM candidates [44], and we concentrate on the annihilation signal. However, we stress that the approach presented here could be extended to any search for DM or other exotic particles if they inject $e^\pm$ in the interstellar medium through annihilation and/or decay processes.

The source term for $e^\pm$ produced from (Majorana fermions) WIMP annihilations in the Milky Way DM halo reads as

$$q_{e^\pm}(\boldsymbol{x}, E) = \frac{1}{2}\left[\frac{\rho_{\rm DM}(\boldsymbol{x})}{m_{\rm DM}}\right]^2 \Sigma_f \langle\sigma v\rangle_f \frac{dN^f_{e^\pm}}{dE}, \tag{1}$$

where $m_{\rm DM}$ is the DM mass, $\rho_{\rm DM}(\boldsymbol{x})$ is the DM density profile in the Galaxy (assumed to be spherically symmetric), f runs over the considered DM annihilation channels, $\langle\sigma v\rangle$ is the velocity averaged cross section, and $dN^f_{e^\pm}/dE$ is the $e^\pm$ energy spectrum per annihilation for each annihilation channel f.

The DM radial distribution $\rho_{\rm DM}(r)$ in the Galaxy at distance r from the halo center can be effectively described by the Navarro-Frenk-White and generalized Navarro-Frenk-White density profile [45,46], where we fix the scale radius to $r_S = 23$ kpc and enforce the local DM density at the solar position to be $\rho_{\rm DM}(r_\odot = 8.5\ {\rm kpc}) = 0.4\ {\rm GeV/cm^3}$ [47]. To estimate the uncertainties related to the DM radial distribution, particularly relevant for the innermost part, we also consider two additional cases [37]. To avoid numerical divergences at $r \to 0$ the profiles are truncated as detailed in Ref. [9]. Contributions connected to the presence of DM substructures on top of the main, smooth halo could boost the total DM annihilation rate, and are conservatively not considered here [48,49].

We consider standard WIMPs with masses $m_{\rm DM}$ between 5 GeV and 1 TeV annihilating into three representative channels: two leptonic channels, $\tau^+\tau^-$ and $\mu^+\mu^-$, expected to produce more $e^\pm$ in their final states, and one hadronic channel $b\bar{b}$, producing a much softer spectrum. The reference thermally averaged annihilation cross section is $\langle\sigma v\rangle = 3\times10^{-26}\ {\rm cm^3\,s^{-1}}$. The $e^\pm$ energy spectrum $dN^f_{e^\pm}/dE$ for each channel is taken from the PPPC4DMID library [50] and includes electroweak corrections [51].

Cosmic-ray propagation and maps.—The propagation of $e^\pm$ in the interstellar medium can be described through a transport equation that can be solved semianalytically [52] or numerically by different means [53]. We here use GALPROP version v54r2766 [54] as adapted in Ref. [9,55] to numerically solve the transport equation and predict the all-sky synchrotron signal maps from DM annihilations. In particular, the computation of the total synchrotron intensity and polarization amplitude is based on the GALPROP developments described in Refs. [21,27], and includes free-free absorption, which is however expected to be subdominant at Planck frequencies. GALPROP can solve the transport equation both in two and three spatial dimensions. Since the GMFs we consider are intrinsically 3D, the 3D implementation has to be used to obtain correct predictions. We employ a spatial resolution of 200 pc in each spatial dimension.

To gauge the uncertainties related to propagation we consider three propagation models taken from the literature [37]. We employ as a benchmark the plain diffusion model without convection and reacceleration (named “PDDE”). References [29,56] found this model to be in agreement with cosmic-ray, synchrotron, and gamma-ray data using a similar GALPROP setup. We test also a model with diffusive reacceleration from the same Refs. [29,56] (named “DRE”), and a model with convection (named “BASE”) from the recent Ref. [57].

We note that GALPROP produces synchrotron maps $\mathcal{J}_{I,P}(\nu, b, l)$ in units of energy^2 × flux, i.e., in units of erg ${\rm cm^{-2}/s/Hz/sr}$, where ν is the frequency and b, l are galactic coordinates. We convert this in “brightness temperature” as

$$T_{I,P}(\nu) = \frac{c^2 \mathcal{J}_{I,P}}{2\nu^2 k_B}, \tag{2}$$

which is the temperature that a body with a RJ spectrum would need in order to emit the same intensity at a given frequency ν. This defines the RJ brightness temperature in units of Kelvins ($K_{\rm RJ}$).

Magnetic field models.—The main systematic uncertainty of the present Letter is anticipated to be associated to the modeling of the GMF, which is still poorly constrained [58]. The magnetic field of our Galaxy is know to have at least two components: a large scale, regular field and an isotropic turbulent, random one. The need for an additional component, called “ordered random” [19] or “striated” [23], has been also recently investigated. This new component corresponds to a large scale ordering of the field, and its intensity is expected to be stronger in the regions between the optical spiral arms. For a comprehensive review on the available tracers, a detailed recap of some current models, and their outstanding issues, we refer the reader to Ref. [58] (and references therein). We thus rely on past studies that fitted the most updated GMF models to multiwavelength data. To bracket the uncertainties associated to GMF modeling, we consider the following three benchmarks: The Sun + 10 model proposed in Refs. [20,59], the model proposed in Ref. [60] (Psh + 11), and the more sophisticated model presented by Jansson and Farrar for the regular [23] and random [24] magnetic fields (JF12) [37].

These models differ both for the regular and the random magnetic field (MF) component. A crucial observation is the fact that intensity and polarization have a different

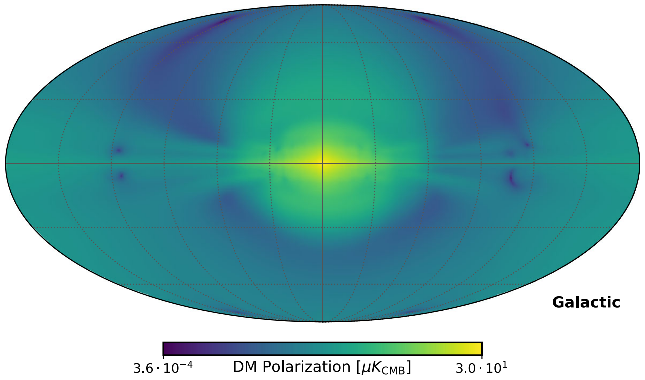

FIG. 2. Polarization amplitude of the synchrotron emission from DM at 30 GHz in units of $K_{\rm CMB}$ as computed for $m_{\rm DM} = 50$ GeV annihilating in $\mu^+\mu^-$ pairs with a thermal averaged cross section of $\langle\sigma v\rangle = 3\times10^{-26}$ cm^3 s^{-1}, and using the PDDE propagation and the Psh + 11 GMF model. The sky map is computed for NSide = 128 and is shown in Mollweide projection.

dependence on the MF. While intensity depends on the total MF (random + ordered), polarization only depends on the regular component. This makes the two probes highly complementary.

Dark matter signal and constraints.—To illustrate the morphology of the polarization DM signals, we show in Fig. 2 the polarization amplitude at 30 GHz for one GMF model (Psh + 11). The map is computed for a DM particle of $m_{\rm DM} = 50$ GeV annihilating into $\mu^+\mu^-$ pairs with $\langle\sigma v\rangle = 3\times10^{-26}$ cm^3 s^{-1}, using the PDDE propagation and for NSide = 128. The polarization amplitude of the DM signal is, as expected, peaked at the Galactic center and extends away from the plane following the morphology of the regular magnetic field in the Milky Way disk and halo from Psh + 11.

We have validated our results comparing the synchrotron DM maps and spectra with previous works [9,10], finding similar results when computing the DM signal within the same setup, when possible. We refer to [37] for more examples of the intensity and polarization DM signal maps.

In the following we use Planck LFI maps at 30 GHz as reference, while we show results using higher frequency maps in [37]. For each simulated DM map, i.e., for each DM mass and annihilation channel, we compute an upper bound on the DM annihilation cross section by requiring that the DM intensity or polarization signal at a given frequency does not exceed the observed Planck signal *plus* the error estimated before, in this way producing limits at the 68% confidence level. We enforce this requirement in each pixel at $|b| < 30°$, and we provide the upper limit corresponding to the most constraining pixel.

As a preliminary step, we study the effect of pixel size [37]. With a small pixel we are sensitive to the detailed morphology of the signal, but the noise per pixel is large, while with a large pixel we have a smaller noise but we lose the details of the morphology. We find that the constraints are optimized for a choice of an NSide = 128, that we adopt in the following [37].

Our results for the upper limits obtained using Planck intensity and polarization data are illustrated in Fig. 3 (left) for different GMF models and for the $\bar{b}b$ channel and PDDE propagation setup. At fixed GMF model, we find that the polarization maps are more constraining than the intensity maps by almost 1 order of magnitude for DM masses larger than 20 GeV. The Sun + 10 and Psh + 11 models use the same parametrizations and intensity values

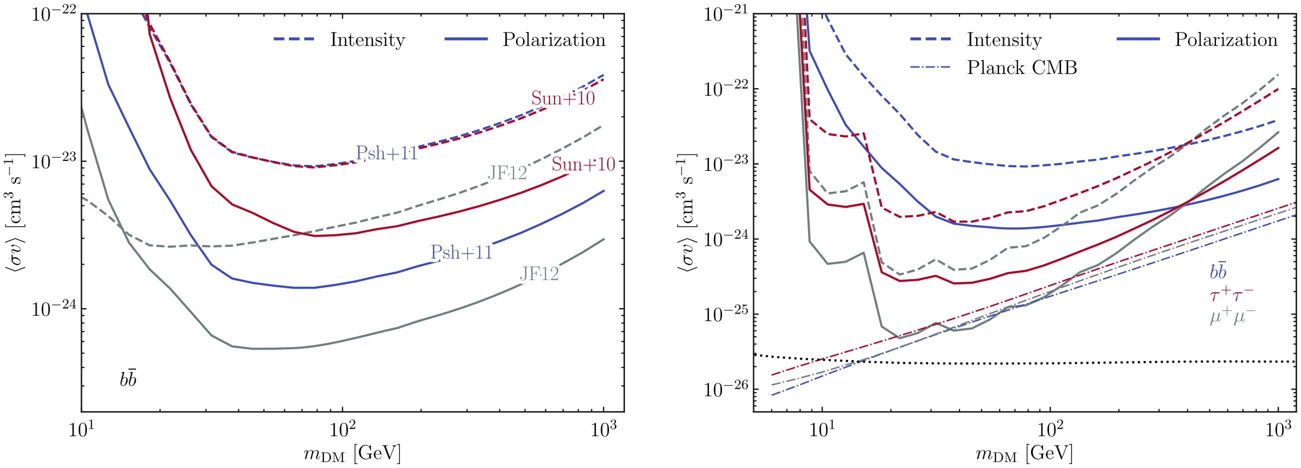

FIG. 3. Upper limits on the thermally averaged annihilation cross section as a function of DM mass as derived from the Planck intensity (dashed lines) and polarization (solid lines) data at 30 GHz. Left panel: effect of the GMF model for the $\bar{b}b$ channel. Right panel: results for different annihilation channels assuming the Psh + 11 GMF model. Results obtained from Planck CMB data [61] are reported as dot-dashed lines for comparison. The dotted line indicates the thermal relic cross section [62]. Note the different y scales in the two panels.

for the random field, and thus the intensity constraints are very similar. The random field of the JF12 model has instead a more complicated morphology and a larger strength, which translates into stronger limits by a factor of 2. The different morphology and strength for the ordered GMF translate into an uncertainty of about 1 order of magnitude in the upper limits obtained with the polarization data. The JF12 model is in this case associated to the most stringent upper limits given the nonzero striated component included. We recall that the strength of the GMF is highly degenerate with the normalization of the CR $e^{\pm}$ density in the Galaxy, and a consistent assessment of the parameters of the GMFs should contextually fit also the CR $e^{\pm}$ injection and propagation parameters. We leave this assessment to future work, in which potentially stronger constraints can be derived by modeling and subtracting the astrophysical Galactic synchrotron emission within the same framework.

The upper limits corresponding to the three annihilation channels $\bar{b}b$, $\mu^+\mu^-$, $\tau^+\tau^-$ are illustrated in Fig. 3 (right) for a fixed choice of Psh + 11 GMF and PDDE propagation setup. The limits reach approximately the same value at about 500 GeV, where the synchrotron emission spectrum from DM annihilations at 30 GHz has similar values for all channels. For all channels, the synchrotron polarization data provide constraints at least a factor of 5 better than the intensity. For different MF (left panel), this is valid for $m_{\mathrm{DM}} > 40$ GeV. At tens of GeV and for $\mu^+\mu^-$ annihilations, we exclude $\langle\sigma v\rangle$ larger than about $10^{-25}\ \mathrm{cm}^3\,\mathrm{s}^{-1}$. This is compared to the thermal relic cross section [62] shown as a dotted line. For the $\mu^+\mu^-$ channel, our upper limits using Planck polarization are competitive with Planck CMB constraints [61] (dot-dashed lines) between about 50 and 100 GeV. We interpret the stronger DM constraints from polarization as coming from two effects. First, the astrophysical backgrounds are lower in polarization rather than in the intensity [37]. Second, the intensity and polarization maps have significantly different morphologies. In particular, as can be seen in Fig. 1, the polarization map presents filaments, or arms, extending many degrees in the sky. This leaves interarms regions with very low background very close to the Galactic center, where the DM signal peaks. Instead, the background for the intensity has a more uniform structure toward the inner Galaxy. While these limits on WIMPs are weaker overall than some other constraints available in the literature [63–69], the conservative analysis presented in this Letter is the first step toward a more detailed assessment of the constraining power of polarization data when the astrophysical background will also be included.

Further systematic uncertainties related to the choice of the propagation setup or the DM radial profile are discussed in [37].

Conclusions.—This Letter presents a new method to constrain DM properties using for the first time the map of CMB foreground polarization as an observable. We have derived new, conservative (i.e., removing only the CMB) DM constraints using Planck synchrotron microwave polarization sky maps. We obtain competitive bounds on the WIMP annihilation cross section, while we find that polarization maps provide DM limits up to 1 order of magnitude stronger than the ones coming from intensity maps. Our method could be generalized to other types of particles with electromagnetic annihilation or decay products. The bounds could be straightened by a proper removal of astrophysical foregrounds on top of the CMB background, by a more accurate modeling of the GMF and of the DM density profile, and finally by more sensitive full-sky observations of the polarized millimeter sky (which should be delivered by the LiteBird satellite [70]).

We thank Michael Krämer for insightful discussion in the initial stages of this work and GALPROP developers for useful conversation. We also thank Fabio Finelli and Andrea Zacchei for providing further insight on the Planck low frequency instrument maps. The work of A. C. is supported by "Departments of Excellence 2018-2022" grant awarded by the Italian Ministry of Education, University and Research (MIUR) L. 232/2016; research grant "The Dark Universe: A Synergic Multimessenger Approach" No. 2017X7X85K, PRIN 2017, funded by MIUR; research grant TAsP (Theoretical Astroparticle Physics) funded by INFN. Simulations were performed with computing resources granted by RWTH Aachen University.

---

[*] Corresponding author.
manconi@physik.rwth-aachen.de

[1] P. Blasi, A. V. Olinto, and C. Tyler, Astropart. Phys. **18**, 649 (2003).

[2] D. Hooper, Phys. Rev. D **77**, 123523 (2008).

[3] E. Borriello, A. Cuoco, and G. Miele, Phys. Rev. D **79**, 023518 (2009).

[4] M. Regis and P. Ullio, Phys. Rev. D **80**, 043525 (2009).

[5] T. Delahaye, C. Boehm, and J. Silk, Mon. Not. R. Astron. Soc. **422**, L16 (2012).

[6] N. Fornengo, R. A. Lineros, M. Regis, and M. Taoso, J. Cosmol. Astropart. Phys. 01 (2012) 005.

[7] Y. Mambrini, M. H. G. Tytgat, G. Zaharijas, and B. Zaldivar, J. Cosmol. Astropart. Phys. 11 (2012) 038.

[8] T. Bringmann, M. Vollmann, and C. Weniger, Phys. Rev. D **90**, 123001 (2014).

[9] A. E. Egorov, J. M. Gaskins, E. Pierpaoli, and D. Pietrobon, J. Cosmol. Astropart. Phys. 03 (2016) 060.

[10] M. Cirelli and M. Taoso, J. Cosmol. Astropart. Phys. 07 (2016) 041.

[11] A. Tasitsiomi, J. M. Siegal-Gaskins, and A. V. Olinto, Astropart. Phys. **21**, 637 (2004).

[12] S. Colafrancesco, S. Profumo, and P. Ullio, Astron. Astrophys. **455**, 21 (2006).

[13] B. B. Siffert, A. Limone, E. Borriello, G. Longo, and G. Miele, Mon. Not. R. Astron. Soc. **410**, 2463 (2011).

[14] N. Fornengo, R. Lineros, M. Regis, and M. Taoso, Phys. Rev. Lett. **107**, 271302 (2011).

[15] E. Carlson, D. Hooper, T. Linden, and S. Profumo, J. Cosmol. Astropart. Phys. 07 (2013) 026.

[16] M. Regis, S. Colafrancesco, S. Profumo, W. J. G. de Blok, M. Massardi, and L. Richter, J. Cosmol. Astropart. Phys. 10 (2014) 016.

[17] D. Hooper, A. V. Belikov, T. E. Jeltema, T. Linden, S. Profumo, and T. R. Slatyer, Phys. Rev. D **86**, 103003 (2012).

[18] N. Fornengo, R. A. Lineros, M. Regis, and M. Taoso, J. Cosmol. Astropart. Phys. 04 (2014) 008.

[19] T. R. Jaffe, J. P. Leahy, A. J. Banday, S. M. Leach, S. R. Lowe, and A. Wilkinson, Mon. Not. R. Astron. Soc. **401**, 1013 (2010).

[20] X. H. Sun, W. Reich, A. Waelkens, and T. Enslin, Astron. Astrophys. **477**, 573 (2008).

[21] A. W. Strong, E. Orlando, and T. R. Jaffe, Astron. Astrophys. **534**, A54 (2011).

[22] T. Bringmann, F. Donato, and R. A. Lineros, J. Cosmol. Astropart. Phys. 01 (2012) 049.

[23] R. Jansson and G. R. Farrar, Astrophys. J. **757**, 14 (2012).

[24] R. Jansson and G. R. Farrar, Astrophys. J. Lett. **761**, L11 (2012).

[25] G. Di Bernardo, C. Evoli, D. Gaggero, D. Grasso, and L. Maccione, J. Cosmol. Astropart. Phys. 03 (2013) 036.

[26] P. Mertsch and S. Sarkar, J. Cosmol. Astropart. Phys. 06 (2013) 041.

[27] E. Orlando and A. Strong, Mon. Not. R. Astron. Soc. **436**, 2127 (2013).

[28] Planck Collaboration, Astron. Astrophys. **596**, A103 (2016).

[29] E. Orlando, Mon. Not. R. Astron. Soc. **475**, 2724 (2018).

[30] L. Jew and R. Grumitt, Mon. Not. R. Astron. Soc. **495**, 578 (2020).

[31] N. Aghanim *et al.* (Planck Collaboration), Astron. Astrophys. **641**, A1 (2020).

[32] Y. Akrami *et al.* (Planck Collaboration), Astron. Astrophys. **641**, A4 (2020).

[33] http://pla.esac.esa.int/pla/#maps, files named LFI_CompMap_Foregrounds-nilc-0XX_R3.00.fits, where XX stands for the frequency channel of 30,44,70 GHz.

[34] The total number of pixels in the map is related to NSide as $N_{\rm pix} = 12\ {\rm Nside}^2$.

[35] K. M. Górski, E. Hivon, A. J. Banday, B. D. Wandelt, F. K. Hansen, M. Reinecke, and M. Bartelman, Astrophys. J. **622**, 759 (2005).

[36] The relation between the brightness temperature and the flux is recalled in Eq. (2); see also Eq. (S3).

[37] See Supplemental Material at http://link.aps.org/supplemental/10.1103/PhysRevLett.129.111103, which includes Refs. [38–42], Sec. I for details on data processing; Sec. II for modeling of the synchrotron emission from Galactic DM: density profile, cosmic-ray propagation, and GMF models adopted; Sec. III for extended results on DM signal (maps and spectra) and on DM constraints, varying pixel size, DM density profile, propagation parameters, Planck frequencies, and for comparisons with other works.

[38] M. Benito, A. Cuoco, and F. Iocco, J. Cosmol. Astropart. Phys. 03 (2019) 033.

[39] S. Murgia, Annu. Rev. Nucl. Part. Sci. **70**, 455 (2020).

[40] A. Burkert, Astrophys. J. Lett. **447**, L25 (1995).

[41] https://sourceforge.net/projects/galprop/.

[42] M. Aguilar *et al.*, Phys. Rep. **894**, 1 (2021).

[43] In the vicinity of sharp features, like point sources, our method is expected to be biased and to return an error estimate larger than the true one. Nonetheless, this does not affect the final results since pixels with a large error will not contribute to constrain DM.

[44] L. Roszkowski, E. M. Sessolo, and S. Trojanowski, Rep. Prog. Phys. **81**, 066201 (2018).

[45] J. F. Navarro, C. S. Frenk, and S. D. M. White, Astrophys. J. **462**, 563 (1996).

[46] J. F. Navarro, A. Ludlow, V. Springel, J. Wang, M. Vogelsberger, S. D. M. White, A. Jenkins, C. S. Frenk, and A. Helmi, Mon. Not. R. Astron. Soc. **402**, 21 (2010).

[47] P. F. de Salas and A. Widmark, Rep. Prog. Phys. **84**, 104901 (2021).

[48] S. Ando, T. Ishiyama, and N. Hiroshima, Galaxies **7**, 68 (2019).

[49] T. Ishiyama and S. Ando, Mon. Not. R. Astron. Soc. **492**, 3662 (2020).

[50] M. Cirelli, G. Corcella, A. Hektor, G. Hutsi, M. Kadastik, P. Panci, M. Raidal, F. Sala, and A. Strumia, J. Cosmol. Astropart. Phys. 03 (2011) 051; 10 (2012) E01.

[51] P. Ciafaloni, D. Comelli, A. Riotto, F. Sala, A. Strumia, and A. Urbano, J. Cosmol. Astropart. Phys. 03 (2011) 019.

[52] D. Maurin, Comput. Phys. Commun. **247**, 106942 (2020).

[53] M. Hanasz, A. Strong, and P. Girichidis, Living Rev. Comput. Astrophys. **07**, 02 (2021).

[54] Publicy available at https://gitlab.mpcdf.mpg.de/aws/galprop.

[55] Publicy available at https://github.com/a-e-egorov/GALPROP_DM.

[56] E. Orlando, Phys. Rev. D **99**, 043007 (2019).

[57] M. Korsmeier and A. Cuoco, Phys. Rev. D **103**, 103016 (2021).

[58] T. Jaffe, Galaxies **7**, 52 (2019).

[59] X.-H. Sun and W. Reich, Res. Astron. Astrophys. **10**, 1287 (2010).

[60] M. S. Pshirkov, P. G. Tinyakov, P. P. Kronberg, and K. J. Newton-McGee, Astrophys. J. **738**, 192 (2011).

[61] N. Aghanim *et al.* (Planck Collaboration), Astron. Astrophys. **641**, A6 (2020); **652**, C4(E) (2021).

[62] G. Steigman, B. Dasgupta, and J. F. Beacom, Phys. Rev. D **86**, 023506 (2012).

[63] A. Albert *et al.* (Fermi-LAT, DES Collaborations), Astrophys. J. **834**, 110 (2017).

[64] R. K. Leane, T. R. Slatyer, J. F. Beacom, and K. C. Y. Ng, Phys. Rev. D **98**, 023016 (2018).

[65] F. Calore, P. D. Serpico, and B. Zaldivar, J. Cosmol. Astropart. Phys. 10 (2018) 029.

[66] M. Regis *et al.*, J. Cosmol. Astropart. Phys. 11 (2021) 046.

[67] A. Cuoco, M. Krämer, and M. Korsmeier, Phys. Rev. Lett. **118**, 191102 (2017).

[68] F. Kahlhoefer, M. Korsmeier, M. Krämer, S. Manconi, and K. Nippel, J. Cosmol. Astropart. Phys. 12 (2021) 037.

[69] F. Calore, M. Cirelli, L. Derome, Y. Genolini, D. Maurin, P. Salati, and P. D. Serpico, SciPost Phys. **12**, 163 (2022).

[70] M. Hazumi *et al.* (LiteBIRD Collaboration), Proc. SPIE Int. Soc. Opt. Eng. **11443**, 114432F (2020).